BALLISTIC ANALYSIS OF NEW MILITARY GRADE MAGNESIUM ALLOYS FOR ARMOR APPLICATIONS

Tyrone L. Jones[1], Katsuyoshi Kondoh[2]

[1]U.S. Army Research Laboratory; APG, MD 21005-5066, USA

[2]Joining and Welding Research Institute (JWRI), Osaka University; 11-1 Mihogaoka; Ibaragi, Osaka, 567-0047, Japan

Abstract

Since 2006, the U.S. Army has been evaluating magnesium (Mg) alloys for ballistic structural applications. While Mg-alloys have been used in military structural applications since WWII, very little research has been done to improve its mediocre ballistic performance. The Army's need for ultra-lightweight armor systems has led to research and development of high strength, high ductility Mg-alloys. The U.S. Army Research Laboratory contracted through International Technology Center-Pacific Contract Number FA-5209-09-P-0158 with the Joining and Welding Research Instituteof Osaka University to develop the next generation of high strength, high ductility Mg-alloys using a novel Spinning Water Atomization Process for rapid solidification. New alloys AMX602 and ZAXE1711 in extruded bar form were characterized for microstructure, mechanical, and ballistic response. Significant increases in ballistic performance were evident when compared to the baseline alloy AZ31B.

Introduction

The U. S. Army Research Laboratory's (ARL) ballistic assessment of magnesium (Mg) alloys over the last 5 years has led to an increased understanding of the material's failure mechanisms and relationship between Mg alloy strength and ductility requirements for lightweight armor applications [1]. While Mg alloys have been used for military structural applications since WWII, very little research has been done to improve its mediocre ballistic performance [2]. The highest strength commercial Mg alloy available in plate form, AZ31B, has proven to be a very good substitute armor material for AA5083 against armor-piercing projectiles on an equal weight basis [3]. It is an adequate substitute armor material against fragment simulating projectiles (FSPs) within an areal density range that is FSP dependent [4]. The ballistic data generated by ARL was used to develop the first set of Mg alloy acceptance standards, MIL-DTL-323333 (MR), titled, "Armor Plate, Magnesium Alloy, AZ31B, Applique" [5]. Ultimate tensile strength (UTS), tensile yield strength (YTS), ductility, and grain size are all key performance parameters in determining the ballistic performance of metals. The bulk material properties of AZ31B are shown in Table I. Figure 1 correlates impact energy absorption (J) vs. Mg armor alloy AZ31B grain size (μm) [6].

In 2009, ARL collaborated with the Joining and Welding Research Institute (JWRI) of Osaka University under contract through International Technology Center-Pacific to develop and evaluate high-strength, high-ductility Mg alloy plate for structural applications. Initial evaluation of conventionally rolled AZ31B plate versus powder formed AZ31B plate showed that grain refinement is not the only parameter that is needed to significantly improve the viability of Mg armor alloy plate [7].
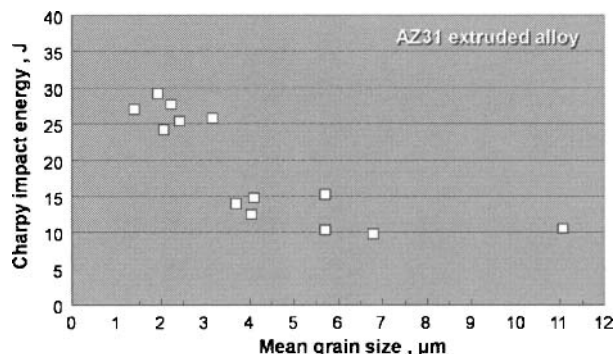

Figure 1. AZ31B Grain Size versus Impact Energy Absorption.

New fundamental Mg alloying is needed to increase the impact energy and thus the performance of Mg alloy plates. The result showed a research opportunity to make Mg alloys a viable armor material that could compete with current aluminum armor alloy solutions [4]. Based on our preliminary material and ballistic analysis, the ARL/JWRI program set goals to develop Mg alloys with the mechanical properties shown in Table I.

Table I. Mechanical Properties/Goals of Mg Alloys

	Ultimate Tensile Strength (MPA)	Tensile Yield Strength (MPA)	Elongation to Failure (%)
AZ31B [7]	245	150	7
New Mg Alloy	400	350	20

Clearly, there were two potential paths forward towards achieving these set goals:

1. Create new chemical compositions to develop high strength, high ductility Mg alloys.
2. Improve grain refinement through novel processing techniques to produce high-strength, high-ductility Mg alloys.

As a result, ARL and JWRI collaboratively developed two new experimental Mg alloys, AMX602 and ZAXE1711, using the advanced metallurgical powder process. The initial material

development and ballistic evaluation of Mg alloy AMX602 and Mg alloy ZAXE1711 are discussed in the next sections.

Material Development

AMX602 (Mg-6Al-0.5Mn-2Ca/mass%) and ZAXE1711 (Mg-1Zn-7Al-1Ca-1La/mass%) Mg alloy powders produced by the Spinning Water Atomization Process (SWAP) were used as raw input materials [8, 9]. The coarse Mg alloy powders were 1-5mm length. It was previously verified that the coarse Mg powders of these lengths were non-combustible. The α-Mg grain size of the raw powders was less than 0.5 μm. The powder compaction and hot extrusion were applied to these raw powders to fabricate the extruded bars. The bar had a cross-section of 24.5 mm x 40 mm x 1000 mm. Tensile test specimens machined from these bars were evaluated at room temperature. The material microstructures were observed using an optical microscope. The microstructural evaluation of ZAXE1711 is withheld from discussion until the patent application is processed.

Experimental Evaluation of Raw materials

In SWAP powder preparation, schematically illustrated in Fig. 2 (a), non-combustive AMX602 magnesium alloy ingots were melted at 1053 K in the ceramic crucible covered with the protection inert gas. Their molten metals were directly streamed inside the spinning water chamber from the crucible nozzle. Table II shows chemical compositions of AMX602 alloy powders prepared by SWAP. The calcium is necessary because it promotes the non-combustive properties of the magnesium alloys. The impurity content of Fe and Cu is s controlled to less than 0.005% because they are corrosive elements in magnesium alloys. As shown in Figure 2 (b), a length of the coarse AMX602 powders prepared by SWAP is 1 ~ 4 mm, and they have an irregular shape. The cast ingot with the same composition was also prepared as a reference input material.

Powder Consolidation

The powder was consolidated at room temperature using a 2000kN hydraulic press machine to fabricate the green compact. The green compact had a relative density of 85% and 42 mm diameter. The columnar compact and cast ingot were heated at 573 ~ 673K for 180 seconds in an argon gas atmosphere, then immediately consolidated into full density material by hot extrusion. An extrusion ratio of 37 and an extrusion speed 1 m/s were used in this study.

Table II. Chemical Compositions of Non-Combustive Magnesium Alloy Powders.

Al	Zn	Mn	Fe	Si	Cu	Ca	Mg
6.01	0.007	0.26	0.002	0.038	0.004	2.09	Bal.

Microstructural Analysis

Figure 3 indicates optical microstructures of AMX602 cast ingot (a), as-received fine powders less than 0.5 mm (b) and coarse powders over 1 mm (c) prepared by SWAP. The cast ingot

material consists of coarse α-Mg grains of 60 ~ 150 μm diameter, and some intermetallic compounds are observed at their grain boundaries.
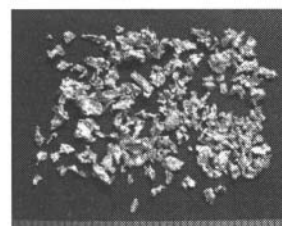
(a)
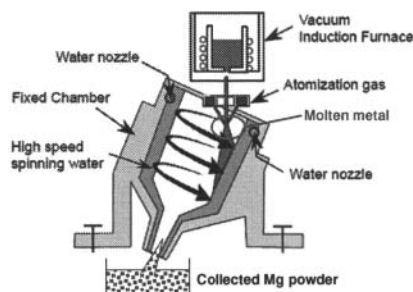
(b)

Figure 2. (a) Schematic Illustration of SWAP Equipment to Produce Rapidly Solidified Mg Alloy Powders; (b) Morphology of Coarse Magnesium Alloy Powder Prepared by SWAP.

As shown in Figure 3(b), the fine powders revealed small dendrite structures that were formed during the rapid solidification of molten Mg alloy droplets after atomization. A mean Dendrite Arm Spacing (DAS) of fine powders Figure 3(b) was 0.97 μm. The coarse powders shown in Figure 3(c) indicate large grains of 4 ~ 8 μm diameter that were caused by a slower solidification rate during atomization. The mean grain size was 6.7 μm. The DAS value was estimated using the following Equation 1 [9], the DAS value suggests the estimated solidification rate (R) of the fine AMX602 powders:

$$\lambda = 35.5R^{-0.31} \qquad (1)$$

where,

λ = DAS (μm),

R = Solidification rate (K/s)

Hence the estimated solidification rate of fine SWAP Mg alloy powders is 1.1×10^5 K/s. The estimated solidification rate of coarse SWAP Mg alloy powders is 6.8×10^3 K/s. The mean particle size of fine and is 0.36 mm. The mean particle size of coarse powders is 1.87 mm. Theses particle sizes are significantly larger than other alloy powders that with 100 ~ 200 μm via the conventional atomization process. This indicates that SWAP Mg alloy powders are very safe in handling. Additionally the SWAP powders showed very fine microstructures due to the high solidification rate of the SWAP. On the other hand, the cast AMX602 alloy had a very small solidification rate of 0.6 K/s calculated by Equation 1. This cast solidification rate was equivalent to the solidification rate for conventional cast Mg alloys [10]. Additionally, the high

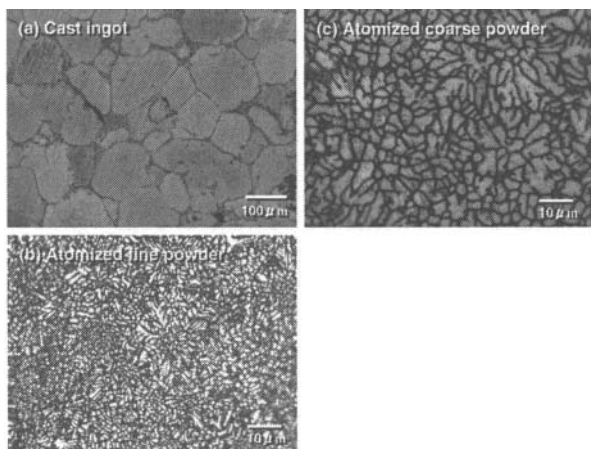rapid solidification rate makes inter-metallic compounds nearly undetectable at the grain boundaries.

Figure 3. Optical Microstructures of Input Raw Materials: (a) As-Cast Ingot Billet; (b) As-Received Fine SWAP Powder; (c) Coarse Powder.

Figure 4 shows differential thermal analysis (DTA) profiles of the atomized coarse powders and cast ingot. The break on the slope at 723 K in both profiles are caused by changing the heating rate from 10 to 5 K/min. The large endothermic peaks were detected at 798 ~ 800 K at both rates, and correspond to a melting point of Al_2Ca intermetallics [8]. Based on these results, the extrusion temperature of the atomized powders and cast ingot should be controlled less than the melting point of Al_2Ca intermetallics at 798 K. In this study, the pre-heating temperature of the green compact and cast ingot material is set at 573 ~ 673 K.
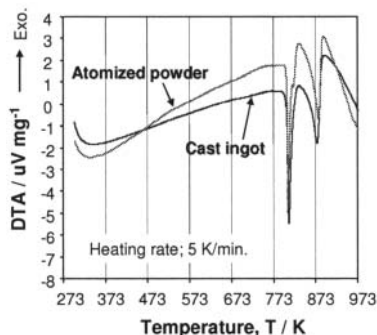

Fig. 4. DTA Profiles of AMX602 Cast Ingot Billet and As-Received Coarse SWAP Powder.

The non-combustive AMX602 magnesium alloys were fabricated by extruding the green compacts of rapidly solidified coarse powders with 1~4 mm via SWAP. They showed extremely fine α-Mg grains of 0.3~1.1μm in diameter via dynamic recrystallization. Fine Al_2Ca compounds with a particles size of 100~300 nm were precipitated during hot extrusion, and uniformly distributed in the matrix. Compared to the AMX602 extruded alloys using the cast ingot billets, TS and YS of the powder extruded materials showed the significant increment of 30~45%. The optimization of the pre-heating temperature before hot extrusion was effective to form very fine recrystallizedα-Mg grains and intermetallic dispersoids.

For example, a good balance of 422 MPa TS and 14.2% elongation was obtained when employing the pre-heating temperature at 623 K.

Figure 5 shows x-ray diffraction patterns of the input raw material and its extruded alloys at 573 K and 673 K. In the case of SWAP powders shown in (a), magnesium oxide (MgO) peak is detected at $2\theta = 43°$, which is caused by oxidation of molten Mg alloy droplets during water atomization. MgO films covering the powder surfaces are thermally stable. It is, however, easy to break them by applying a very low pressure in consolidation because of their porous structures [11]. No Al_2Ca intermetallic peak is shown in the profile of the raw powder, but it is detected in the extruded alloys. This means that Al and Ca are solid-soluted in the matrix of the as-received raw powder by rapid solidification. However, Al_2Ca compounds are precipitated due to the high elevated temperature during hot extrusion. The peak intensity of Al_2Ca gradually increases with increase in the extrusion temperature. That is, the amount of precipitated Al_2Ca intermetallics increases by a larger thermal history in pre-heating. On the other hand, as shown in (b), the cast ingot material before extrusion originally contains coarse Al_2Ca intermetallics crystallized during casting [12]. There is no remarkable difference of the profile of the wrought alloys extruded at between 573K and 673K.
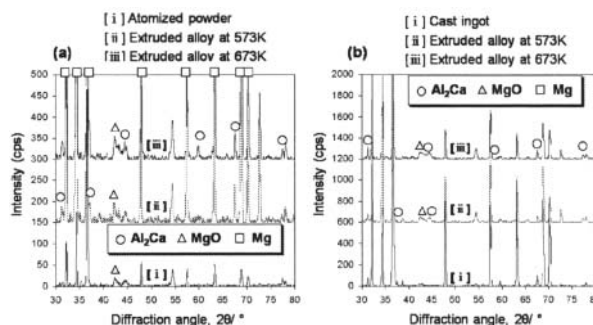

Fig. 5. X-Ray Diffraction patterns of Input Raw Material and AXM602 Alloys Extruded at 573 K and 673 K using SWAP: (a) Powder Compact; (b) Cast Ingot Billet.

Figure 6 reveals SEM observation results on the extruded AMX602 alloys by using the powder compact (a) and cast ingot billet (b). The extrusion temperature is 573 K and 673 K. The powder extruded materials shows extremely fine grains of 0.3 ~ 1.1 μm in diameter, compared to the cast ingot extruded ones shown in (b). With regard to the effect of the extrusion temperature on the grain size of the powder extruded material, the mean grain size of the wrought alloy at 573 K calculated by the image scanning soft ware is 0.45 μm, and that of the extruded alloy at 673 K is 0.8 μm. The larger thermal history during pre-heating in the latter at 673 K causes a small grain growth after dynamic recrystallization in hot extrusion [13]. The amount of precipitated Al_2Ca intermetallic compounds, which correspond to white fine particles of 100 ~ 300 nm distributed in the matrix, of the extruded alloy at 673 K is larger than that of the wrought alloy at 573 K. On the other hand, Fig. 6 (b-1) indicates that the AMX602 wrought alloy extruded at 573 K using the cast ingot billet consists of fine α -Mg grains of 1 ~ 3 μm via dynamic recrystallization. Some of large grains of 5 ~ 10 μm are observed in the matrix. The mean grain size of the extruded materials at 573

K is 1.96 μm. However, when employing the higher pre-heating temperature at 673 K, a lot of coarse grains over 10 μm exist in the matrix as shown in (b-2) and a few fine grains less than 3 μm are observed. The mean grain size is 3.29 μm. Compared to the microstructure shown in (b-1), the grain growth and coarsening of (b-2) certainly occurred during extrusion at higher temperature of 673 K after dynamic recrystallization. Both wrought alloys using cast ingots contain coarse intermetallic compounds with irregular morphologies. Compared to AMX602 cast ingot material, some small compounds are observed because severe plastic deformation during hot extrusion caused fragmentation of coarse and brittle intermetallics distributed in the matrix.
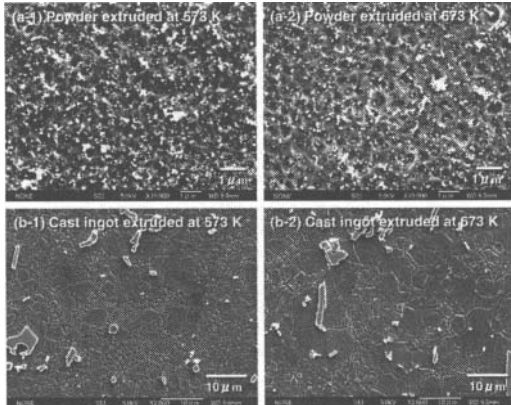

Figure 6. Scanning electron microscope observation on AMX602 alloys extruded 573 K and 673 K using SWAP powder compact (a) and cast ingot billet (b).

Figure 7 shows a micro hardness dependence on the grain size of the extruded AMX602 alloys fabricated by using SWAP powder compacts and cast ingot billets. Micro-Vicker's hardness of each material shown in Figure 7 is as follows; 113 HV (a-1), 94.3 HV (a-2), 77.0 HV (b-1), and 69.9 HV (b-2). The hardness of wrought alloys using atomized powder compacts is larger than that using the cast ingot. This is due to the extremely fine grains and very small intermetallic compounds of the former materials as mentioned in Figure 7. It reveals that the micro hardness is proportional to $d^{-0.5}$ (d: α -Mg grain size), and Hall-Petch relationship is shown in these data. Figure 9 indicates a dependence of tensile strength (TS) and yield stress (YS) of the extruded AMX602 alloys on the pre-heating temperature. TS and YS of the wrought alloys using the cast ingot billets is 298 ~ 311 MPa and 204 ~ 251 MPa, respectively. It is reported that the content of Ca included AM60 alloys is effective for not only their non-combustive but also mechanical properties because coarse intermetallics of Al_2Ca with irregular shapes cause the decrease of the tensile properties [8, 13]. Therefore, when using the cast ingot billet, the maximum content of Ca is 2 mass%. On the other hand, the alloys using the SWAP powder compacts show an extremely high strength of 391 ~ 452 MPa TS and 358 ~ 428 MPa YS. Concerning their dependence on the temperature, both materials reveal the decrease of TS and YS with increase in the pre-heating temperature due to the grain growth and coarsening as shown in Figure 5. In particular, the decrement of the strength of SWAP powder extruded alloys is larger than that of cast ingot extruded materials. The fine microstructures via dynamic recrystallization of the former are very sensitive to the temperature [14], and the

grain growth by solid-diffusion easily occurs when a higher pre-heating temperature is applied.
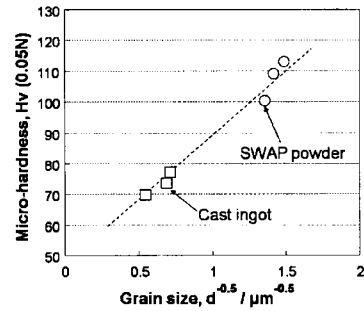

Figure 7. Dependence of micro-Vicker's Hardness on Grain Size of Extruded AMX602 Alloys.

As shown in Figure 8, the elongation increases with increasing the temperature. The SWAP powder extruded alloy at 623 K shows a good balance of 422 MPa TS and 14.2% elongation. As shown in Figure 9, fine dimple fractured patterns, which mean typical fractures inside α-Mg grains, are observed, and no fracture at the primary particle boundaries observed in the by SEM image. The fragmentation of intermetallic compounds at the fractured surface is not observed. Therefore, this material shows a high strength and good ductility. On the other hand, Figure 9 indicates the fractured surface of the cast ingot extruded alloy at 623 K. It also shows dimple fractured patterns. However, the coarse brittle intermetallic compounds include some cracks marked with white arrows, and they correspond to the initiation and propagation of the fracture.
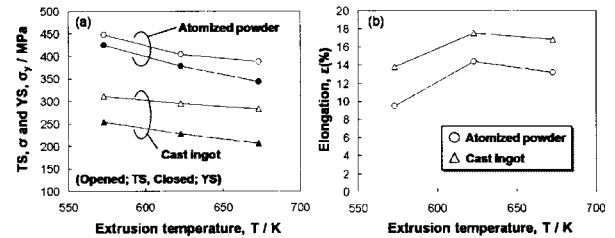

Figure 8. Tensile Strength, Yield Stress and Elongation Dependence on Pre-Heating Temperature.
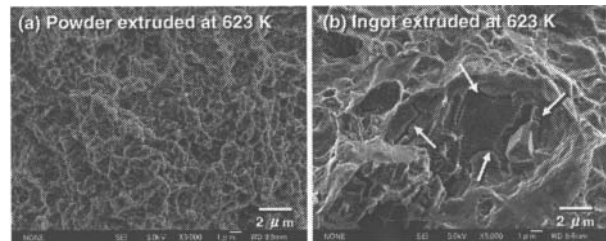

Fig. 9. SEM Observation on Fractured Surface of Tensile Test Specimen of Extruded at 623 K using Powder Compact (a) and Cast Ingot (b).

428

Mechanical Test Results

The mechanical properties of the Mg alloy AMX602 and Mg alloy ZAXE1711 samples are shown in Table III and Table IV. Mg alloy AMX602 and ZAXE1711 bars of three different tempers were produced for ballistic evaluation. Measurements at 0° were taken at the center and 0.25" width of the specimen. The temper designations (i.e. AMX602-temper) for each Mg alloy extrusion temperature were as follows:

For AMX602:	For ZAXE1711:
1: 350°C	B: 350°C
2: 300°C	C: 250°C
3: 250°C	D: 200°C

Table III. Mechanical Properties for Mg Alloy AMX602

	0° - center			0° - 1/4 width			45°			90°		
	σ	σy	El	σ	σy	El	σ	σy	El	σ	σy	El
	MPa	MPa	%	MPa	MPa	%	MPa	MPa	%	MPa	MPa	%
Rod 1	355	301	21.0	359	306	19.2	319	234	18	330	244	16.4
Rod 2	357	314	20.8	363	302	18.0	323	236	22.4	307	237	8.5
Rod 3	358	311	17.8	360	312	19.1	324	261	15.1	304	244	7.6

Table IV. Mechanical Properties for Mg Alloy ZAXE1711

	0° - center			0° - 1/4 width			45°			90°		
	σ	σy	El	σ	σy	El	σ	σy	El	σ	σy	El
	MPa	MPa	%	MPa	MPa	%	MPa	MPa	%	MPa	MPa	%
Rod B	377	268	17.4	380	276	17.4	356	245	15.8	363	248	13.0
Rod C	380	269	18.2	384	280	18.4	361	245	18.7	369	246	18.2
Rod D	388	274	18.7	391	286	18.3	362	238	22.5	374	236	19.4

Note the difference between the mechanical properties of Mg alloy AMX602 and Mg alloy ZAXE1711 at the selected tempers are very small. This means extrusion temperature will not be a significant factor on the mechanical properties of these alloys strength when fabricating the scale-up specimens.

Ballistic Evaluation

Based on the aforementioned MIL-DTL-32333 required baseline thicknesses, the Mg alloy bars were evaluated using the .30-cal. FSP. The test projectile schematic diagram, weights, and hardness specifications are shown in Figure 10 and Table V. The hardness of each Mg alloy test bar was measured using the 500-kg Brinell scale. The nominal hardness of each Mg alloy test bar is shown in Table VI.

Table V. Projectile Weight and Hardness Requirements

FSP Type	Weight (gr)	Rockwell C Hardness
.30 Cal	44.0 ± 0.5	30 ± 1

All V_{50} ballistic limits (velocity at which the projectile is expected to perforate the armor 50% of the time) were calculated following MIL-STD-662F [15] and are shown in Table VI. Mg alloy AMX602 showed to a 33% increase in the V_{50} ballistic limit compared to Mg armor alloy AZ31B (attained from MIL-DTL-

32333), while Mg alloy ZAXE1711 showed to a 37% increase in the V_{50} ballistic limit compared to Mg armor alloy AZ31B.
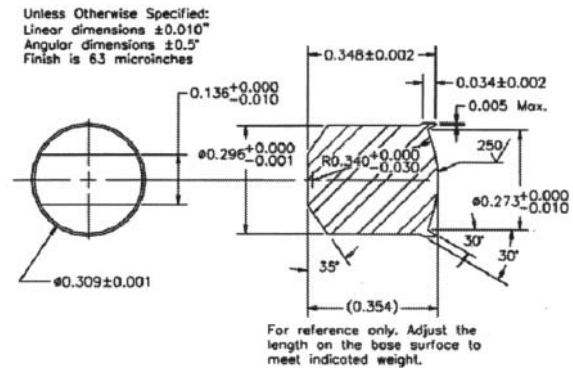

ALL UNITS ARE IN INCHES.

Figure 10. The .30-cal. FSP Schematic Diagram.

The thin plates were held horizontally in a test fixture by C-clamps on the ends of the bars. As evident in figures 11 & 12, the AMX602 showed confined impact. For the instances the projectile perforated the Mg alloy AMX602 bar and created an exit hole, the spall was typically localized within a 31.75-mm diameter. Although the edge of the spall after ballistic impact reached the edge of the AMX602 and ZAXE1711 bars, the V_{50} data significantly exceeded Mg alloy AZ31B V_{50} data at the same areal weight while keeping its structural integrity.

Table VI. Mg Alloy V_{50} Ballistic Velocities

Metal Alloys	Thickness	*Hardness	Ballistic Limit	Ballistic Limit
	mm	HBN	m/s	ft/s
AZ31B	25.400	61	833	2733
AMX602-1	25.190/25.235	80	1061	3480
AMX602-2	25.171/25.210/25.197	80/80/83	1092	3570
AMX602-3	25.171/25.178	80	1105	3624
ZAXE1711-B	25.248	80	1111	3646
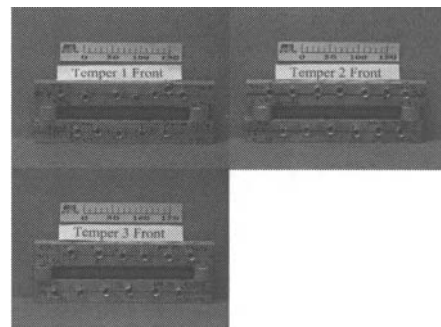
(a) Front
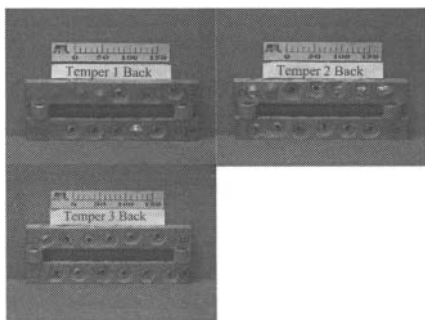
(b) Back

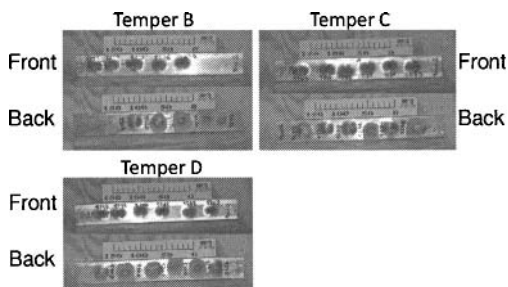Figure 13. Post-ballistic pictures of Mg alloy AMX602 bars.

Figure 14. Post-ballistic pictures of Mg alloy ZAXE1711 bars.

Conclusions

The non-combustive AMX602 magnesium alloys were fabricated by extruding the green compacts of rapidly solidified coarse powders with 1~4 mm via SWAP. They showed extremely fine α-Mg grains of 0.3~1.1μm in diameter via dynamic recrystallization. Fine Al₂Ca compounds with a particle size of 100 ~ 300 nm were precipitated during hot extrusion, and uniformly distributed in the matrix. Compared to the AMX602 extruded alloys using the cast ingot billets, TS and YS of the powder extruded materials showed the significant increment of 30~45%. The optimization of the pre-heating temperature before hot extrusion was effective to form very fine recrystallized α-Mg grains and intermetallic dispersoids. For example, a good balance of 422 MPa TS and 14.2% elongation was obtained when employing the pre-heating temperature at 623 K.

New Mg alloy AMX602 and Mg alloy ZAXE1711 bars showed superior ballistic performance as an armor alloy when compared to baseline Mg armor alloy AZ31B plate. Through advanced powder metallurgy processing and chemical alloying, superior mechanical properties were achieved. Initial ballistic performance results of Mg alloy AMX602 showed up to a 33% higher ballistic limit compared to the baseline Mg armor alloy AZ31B. Initial ballistic performance results of Mg alloy ZAXE1711 showed up to a 37% higher ballistic limit compared to the baseline Mg armor alloy AZ31B. Future development will include the scaling up of Mg alloy AMX602 bars to plate for further analysis and full scale structural applications. It is expected that the ballistic limit and thus the overall ballistic performance of the scaled size will increase because of the reduction of the edge effects during an impact. Pending successful results of the large scale Mg alloy AMX602 development, Mg alloy ZAXE1711 will follow the same large scale development plan.

References

1. Jones, T.; DeLorme, R.; Burkins, M.; Gooch, W. *Ballistic Evaluation of Magnesium Alloy AZ31B*; ARL-TR-4077; U.S. Army Research Laboratory: Aberdeen Proving Ground, MD, April 2007.
2. Mathaudhu, S.; Nyberg, E.; *Magnesium Alloys in Army Applications: Past, Current and Future Solutions*; Proceedings of the 2010 Minerals, Metals and Materials (TMS) Annual Symposium, Seattle, WA, February 2010.
3. Jones, T.; DeLorme, R.; *Development of a Ballistic Specification for Magnesium Alloy AZ31B*; ARL-TR-4664; U.S. Army Research Laboratory: Aberdeen Proving Ground, MD; December 2008.
4. Jones, T.; DeLorme, R.; *A Comparison of the Ballistic Performance Between Rolled Plate in AZ31B-H24 Magnesium and 5083-H131 Aluminum*; 24th International Symposium on Ballistics, New Orleans, LA; September 2008.
5. MIL-DTL-32333 (MR); Armor Plate, Magnesium Alloy, AZ31B, Applique; 2009.
6. Liao, J.; Hotta, M.; Kaneko, K.; Kondoh, K.; *Enhanced Impact Toughness of Magnesium Alloy by Grain Refinement*; Scripta Materialia 2009, 61; 208-211.
7. Jones, T.; Kondoh, K.; *Initial Evaluation of Advanced Powder Metallurgy Magnesium Alloys for Dynamic Applications*; ARL-TR-4828; U.S. Army Research Laboratory, Aberdeen Proving Ground, MD; May 2009.
8. Sakamoto, M.; Akiyama, S.; Hagio, T.; Ogi, K.; *Control of Oxidation Surface Film and Suppression of Ignition of Molten Mg-Ca Alloy by Ca Addition*; Journal of Japan Foundry Engineering Society; 69 (1997) 227-233.
9. Nishida, S.; Motomura, I.; *Estimation of Heat Transfer Coefficient and Temperature Transition on Melt Drag Process of AZ31 Magnesium Alloy by Heat Transfer and Solidification Analysis*; Journal of Japan Institute of Light Metals; 58 (2008) 439-442.
10. Wei, L. Y.; Dunlop, G. L.; *The Solidification Behavior of Mg-Al-rare Earth Alloys;* Journal of Alloys and Compounds; 232 (1996) 264-268.
11. Šplíchal, Karel; Jurkech, Ludvík; *Comparison of Oxidation of Cast and Sintered Magnesium Materials in CO2*; Journal of Nuclear Materials; 48 (1973) 277-286.
12. Anyanwu, I.A.; Gokan, Y; Suzuki, A.; Kamado, S; Kojima, Y.; Takeda, S.; Ishida, T.; *Effect of Substituting Cerium-Rich mischmetal with Lanthanum on High Temperature Properties of Die-Cast Mg-Zn-Al-Ca-RE alloys*; Materials Science and Engineering A; 380 (2004) 93-99.
13. Chandrasekaran, M.; and John, Y.M.S.; *Effect of Materials and Temperature on the Forward Extrusion of Magnesium Alloys*; Materials Science and Engineering A; 381 (2004) 308-319.
14. Zhang, J.H.; Liu, Hai Feng; Sun, W.; Lu, H.Y.; Tang, D.X.; Meng, Jian; *Influence of Structure and Ionic Radius on Solubility Limit in the Mg-Re Systems*, Materials Science Forum; Vol.561-565 (2007) 143-146; doi10.4028/www.scientific.net/MSF.561-565.143; accessed October 2010.
15. MIL-STD-662F; V_{50} Ballistic Test For Armor; 1997.